SNB-D-17-02603 REVISED

Robust polarization active nanostructured 1D Bragg Microcavities as optofluidic label-free refractive index sensor

M. Oliva-Ramírez[a,1]*, J. Gil-Rostra[a], F. Yubero[a] and A. R. González-Elipe[a]*.

[a]Instituto de Ciencia de Materiales de Sevilla (CSIC-Univ. Sevilla). Avda. Américo Vespucio 149. 41092 Sevilla. Spain.

*Corresponding authors: manuel.oliva@icmse.csic.es; arge@icmse.csic.es.

Keywords: Refractive index sensor; Label free sensor; Optofluidics; GLAD; Oblique Angle Deposited Thin film; Optical retarder transducer.

Abstract:

In this work we report the use of polarization active porous 1D Bragg microcavities (BM) prepared by physical vapor deposition at oblique angles for the optofluidic analysis of liquid solutions. These photonic structures consist of a series of stacked highly porous layers of two materials with different refractive indices and high birefringence. Their operational principle implies filling the pores with the analyzed liquid while monitoring with linearly polarized light the associated changes in optical response as a function of the solution refractive index. The response of both polarization active and inactive BMs as optofluidic sensors for the determination of glucose concentration in water solutions has been systematically compared. Different methods of detection, including monitoring the BM wave retarder behavior, are critically compared for both low and high glucose concentrations. Data are taken in transmission and reflection modes and different options explored to prove the incorporation of these nanostructured transducers into microfluidic systems and/or onto the tip of an optical fiber. This analysis has proven the advantages of the polarization active transducer sensors for the optofluidic analysis of liquids and their robustness even in the presence of light source instabilities or misalignments of the optical system used for detection.

Present address
[1]Leibniz Institute for New Materials. Campus D2 2, PC: 66123 Saarbrücken, Germany.

Abbreviations
Photonic crystals: PC; Bragg Microcavity: BM; Refractive index: RI; Refractive Index Unit: RIU

1 Introduction.

The development of multifunctional "lab on a chip" microfluidic systems requires very sophisticated transducers and robust, cheap and reliable interrogation procedures capable of providing reversible and straightforward detection functions.[1] Photonic crystal (PC) detection systems are very common in microfluidics because of their flexibility, non-destructive character and the rich variety of physical principles available for detection.[2,3] These include many examples related to plasmonic detection.[4–6] In this case, detection can be mediated by the incorporation of specific molecules grafted on the surface of the plasmonic metal (i.e., label-type procedures), an approach that has demonstrated high selectivity and low limit of detection, although the possible degradation of the label molecules usually restricts a prolonged utilization.[4,5]. In more recent works using plasmonic structures made of silver organized in the form of a 2D-PC deposited on a flat silver layer, Liu et al. [6] have shown a redshift of a resonant peak and sensitivity limits for detection of glucose similar to those determined in the present work using a different interrogation strategy. Other PC–based methods rely on optical interferences which are much affected by small changes in optical parameters (e.g., refractive index (RI)) of the interrogated fluids. [14,15] This is for example the basis of optical fibers based PCs consisting of a stack of layered polymers that, experiencing a swelling expansion in the presence of glucose, give rise to changes in transmitted light. [7] Changes in resonances in ring resonators[8] and other optical principles[9,10] constitute the basis of other type of label-free PC integrated microfluidic sensors,[11] in some cases with ultimate capacities of analyzing ultra-small volumes up to the femtoliter level.[12,13] Typical PC configurations include 3D ordered opal photonic sensors,[16] inverse opals [17] and cavities,[18,19] 2D PC waveguides,[20] slotted PC heterostructures,[21] or ordered arrangement of nanopillars.[22]

Recently, we have reported the synthesis and characterization of nanostructured 1D-PCs that, acting as Bragg mirrors, experience a spectral redshift when infiltrated with liquids.[23] This type of PCs consists of a series of stacked porous layers with alternant low and high values of RI that, through optical interferences, give rise to a spectral gap in their transmission spectra. These multilayer structures with porosities up to 50% of their total volume were prepared by Physical Vapor Deposition at Oblique Angles (PV-OAD), a suitable technique for nanoscale tailoring the growth of highly porous thin films and multilayers.[24] Modulation of porosity, RI and nanostructure of PV-OAD stacked multilayers has been a common strategy to build Bragg reflectors made of either one single material (e.g.,TiO_2,[25,26] ITO [27,28] or silicon[29]) or two materials of different RI (e.g., alternating layers of TiO_2 and SiO_2 [30–33]). Porous Bragg Microcavities (BM), incorporating a thicker central layer within the stack and depicting a narrow resonant peak in the middle of the spectral gap, have been also prepared with the same technique.[30,34] The working principle of these 1D porous microcavities is similar to that of 3D hollow microcavities [9,10] or inverse opals [17] for determining the RI of liquids, with the difference that the empty space available for liquid infiltration is provided in this case by the porosity of the constituent layers and not by any hollow zone separating the structural elements.

Using this type of BM, we have shown a resonant peak redshift upon liquid infiltration which, being dependent on liquid RI, was used to determine the concentration of solutions or the proportion of components in mixtures of liquids.[30] Recently, we have also demonstrated that these BMs can be made polarization active and their retarder behavior modulated by liquid infiltration.[34] In these previous publications, we described the performance of the BM device in a proof of concept approach. Herein, this is extended to a systematic analysis of the capabilities of the system to analyze aqueous solutions of technological interest, working in

different experimental geometries (transmission/reflection) and with several evaluation protocols. In particular, we systematically study the possibilities of all possible polarization effects for liquid analysis within the perspective of the microfluidic integration of these BMs as liquid sensors. As case example, we apply the optofluidic transducer behavior of these BMs to analyze in a continuous way the changes in the RI of glucose solutions ranging from low (i.e. smaller than 0.5 M) to very high concentrations (i.e., in the order of 4 M).

Determination of glucose concentrations is a key issue for critical activities related with human health [35] or food industry [36] where its analysis has been accomplished by a large variety of methods including density and RI determination, plasmonic transduction,[4,5] enzymatic[37] or enzymatic/electrochemical detection[38] or pure electrochemical analysis.[39] Generally, these methods are designed to work within either high or low ranges of glucose concentrations and there is not a proper method covering simultaneously both situations. For low glucose concentrations a high sensitivity and a low limit of detection are critical parameters in health related problems.[35] An advantage of the BMs developed in this work is that they can properly monitor at both high and low ranges. Another is that they can be easily integrated within microfluidic devices to work in continuous for long periods or directly attached to the tip of an optical fiber and measurements made in transmission or reflection modes. Moreover, we show that the chips incorporating polarization active BMs can operate with simple and robust LED sources and conventional photodetectors, thus avoiding the use of monochromators and sophisticated light sources. In the present work, besides proving all these features, we have determined the sensitivity and limit of detection for all explored measuring strategies either in the transmission or reflection modes. It has been shown that while the former seems rather adequate for microfluidic integration, the latter could be taken as an immersion procedure for the direct monitoring of liquids in flow lines or containers.

2 Materials and methods

2.1 Materials preparation and characterization

Porous and nanostructured BMs made of stacked TiO_2 and SiO_2 layers were deposited by PV-OAD according to a procedure reported previously.[23,30,34,40] BMs were deposited on quartz plates of 1.25x2.50 cm and on silicon wafers by electron beam evaporation in an oblique angle configuration at a zenithal angle (α) of 70^o. These photonic structures consist of a stack of 15 alternating TiO_2 or SiO_2 porous layers (first and last layer of the multilayer structure made of TiO_2). The thickness of these layers was about 85nm, except for a thicker central layer of SiO_2 of about 200nm, this latter acting as optical defect. The prepared BMs responded to *chiral* and to *zig-zag* morphologies of the nanocolumns forming the structure of the individual layers obtained by OAD. These two kinds of microstructures were obtained by azimuthally turning the substrate from one layer to the next by 90^o or 180^o, respectively. The *zig-zag* microstructure was polarization active and presented wave retarder behavior. Although a full description of the microstructural peculiarities of these samples can be found in ref.[34], for the case of the *zig-zag* microstructure it is of relevance to remind here that its polarization activity is related with the existence of a so called fence-bundling direction that corresponds to a preferential lateral association of nanocolumns in this case. This direction is perpendicular to the incoming flux of material during deposition (for details see Figure S1 in supporting information). The fence-bundling makes the films birefringent, with optical axes parallel (slow axis) and perpendicular (fast axis) to the nanocolumn association direction. This direction will be used as a reference to

orient the polarizers when these optical components are used for the measurements (Figure S1 in supporting information).

Scanning electron microscopy (SEM) cross section micrographs of diced silicon supported BMs were taken in a Hitachi S4800 field emission microscope working at 2 keV primary beam energy. Secondary Electron (SE) and the Back Scattered Electron (BSE) detecting modes were used to highlight either topographic or compositional information, respectively.

2.2 Optofluidic analysis with BMs

Optofluidic analysis upon infiltration of the BMs with water and aqueous solutions of glucose was carried out in homemade microfluidic chips simulating typical channels/cavities in real microfluidic devices. A scheme of this optofluidic chip is presented in Figure 1a. The BM was deposited on a fused silica plate and then covered with another cap plate of silica with two orifices acting as inlet and outlet of liquids. An area larger than $1cm^2$ in the center of the chip was left free for optical analysis. A general assumption is that the liquid fills completely the pore volume of the photonic structure (i.e., approximately 50% of the total volume of the multilayer). A layout scheme of the optical components used for the measurements in transmission and reflection is also reported in Figures 1b and 1c. When using the *chiral* BM no special care must be taken regarding the azimuthal orientation of the multilayer with respect to the polarization plane of light and for simplicity non-polarized light was used for the analysis. Experiments with the *zig-zag* BM were carried out as a function of the linear polarization of light by placing a second polarizer between the detector and the chip, either in transmission or reflection configurations (see Figures 1b & c).

When including this second polarizer in the path of the transmitted or reflected beams, the sample was azimuthally oriented (angle Φ) with the fence-bundling direction forming 45^o with respect to the polarization plane of the excitation beam.[34] A critical analysis justifying this specific azimuthal orientation can be found in a previous work.[34]

According to Figure 1b, normal geometry was used for the measurements in transmission. Spectra were taken in a Cary 100 spectrophotometer. A first series of experiments in transmission geometry with microfluidic chips incorporating the zigzag BM were carried out with linearly polarized light placing a polarizer (pol#1) between the light source and the chip. In these conditions, spectra were recorded with pol#1 oriented parallel to the fence-bundling direction of the zigzag BM (zigzag-∥ configuration) or forming 90^o with respect to it (zigzag-⊥ configuration). Other series of experiments with the *zig-zag* BM were carried out with linearly polarized light obtained by placing the first polarizer (pol#1) between the light source and the microfluidic chip and a second polarizer (pol#2) between the detector and the chip, either in transmission or reflection configurations (see Figures 1b & c). As already said, when including this second polarizer in the path of the transmitted or reflected beams, the sample was azimuthally oriented with the fence-bundling direction forming 45^o with respect to polarization plane of the incident light to maximize the retarder behavior of the multilayer.[34]

Optofluidic analysis in reflection mode was done using a home-made optical set-up employing optical fibers and two turning linear polarizer stages as represented in Figure 1c). The impinging and reflected beam directions were 30^o apart (incidence 15^o off normal). In this layout, the two optical fibers focus on the same spot of the BM layer and the two polarizers can be properly aligned. An image of the whole system is shown in Figure 1d).

For some experiments, the position of the resonant peak before and after liquid infiltration (i.e., to determine the magnitude of redshift) was carefully determined by either a Gaussian fit or at the inflection point of its first derivative.

Based on the capacity of the optical components used for detection and the reproducibility of results, a maximum capacity of detecting concentrations changes of 0.015 M can be assumed (see below). Assuming lineal tendencies at low or high concentration ranges, approximate sensitivity parameters have been determined for each method of detection. These values are approximations because for given concentration ranges not always a well-defined lineal relationship is hold between the monitored optical parameter and the concentration of glucose.

3 Results and Discussion

3.1 Microstructural and Optical characterization of BMs

SEM cross-section micrographs of *chiral* and *zig-zag* BMs are presented in Figure 2 a) and b). The BSE-SEM micrographs in this figure clearly reveal the stacking of the TiO_2 (light grey) and SiO_2 (dark grey) individual layers. Meanwhile, the SE-SEM images illustrate the specific columnar shape of these BMs. The included schemes represent how the orientation of nanocolumns varies from one layer to the next. These BMs are quite porous (ca. 50% void space) and for the *zig-zag* structure the nanocolumns associate laterally defining the already mentioned fence-bundling direction producing the polarization activity and phase retarder behavior to this type of BM (see section 3.2).[34]

UV-vis transmission spectra recorded with unpolarized light for these two BMs are presented in Figures 2c) and d) and are characterized by a single and a double resonant peak, this latter with two components separated by 23 nm, for the *chiral* and *zig-zag* BMs, respectively. The double peak in the latter is an indication of optical activity.[34]

When the BMs were infiltrated with liquids the whole spectra experienced a red shift that can be quantified measuring the resonant peak position. This is clearly observed in the spectra of Figure 2c) & d) when the two porous structures were filled with water. It is noteworthy that the double resonant peak observed in the *zig-zag* BM seemed to coalesce into a single peak after infiltration. A careful analysis with linearly polarized light of the two water infiltrated BMs (Figure S2 in supporting information) reveals that, unlike the single resonant peak characteristic of the *chiral* BM, the slightly broader resonance peak depicted in Figure 2d) for the *zig-zag* BM filled with water is actually composed of two resonant peaks separated by 8 nm.

In a previous work,[34] we showed that the magnitude of redshift and the separation between the two resonant peak components in the *zig-zag* BMs is a function of the RI of the liquid infiltrating the pores. This behavior was accounted for by the substitution of the air filling the BM pores (n=1) by a liquid with n>1. According to the effective medium approximation theory for composite optical systems,[41] changing the RI of one of the phases of a composite system produces a change in the overall RI of the system.

3.2 Monitoring glucose solutions in transmission mode

Three analytical strategies were used in transmission geometry to determine the glucose concentration of the solutions using *chiral* and *zig-zag* BM chips. These strategies consist of measuring i) wavelength shifts (i.e., redshifts) of the resonant peak position, ii) changes in the transmittance at a given wavelength and iii), for the *zig-zag* BMs, changes of the polarization activity. As case examples to prove these three measurement strategies, we have carried out

the analysis of glucose solutions with concentrations ranging from 0.1 M to 4.0 M. Strategies similar to i) and ii) (i.e. measuring redshifts or changes in transmission) have been previously utilized by others to determine glucose concentrations using 2D-PCs.[8] Basic assumption in the present investigation is that the photonic chips respond to the changes in RI associated to the variations of glucose concentration in water solutions.[42]

3.2.1 Determination of glucose concentration measuring redshifts in BMs' resonant peaks.

The infiltration of the BMs with glucose solutions produced a redshift in the resonant peak of the transmitted spectra. Figure 3 presents a series of resonant peak spectra recorded for a chip with a *zig-zag* BM after flowing glucose solutions of varying concentrations from 0.5 to 4.0 M. Similar series of spectra were recorded for the chip with *chiral* BMs (see Figure S3 in supporting information). For the *zigzag* BM, spectra were recorded with the polarization plane of the incoming light oriented parallel to the fence-bundling direction (i.e., *zigzag-∥* configuration) (Figure 3a and 3b). Similar spectra but shifted 8 nm to the red were recorded with linearly polarized light oriented perpendicular to this same fence-bundling direction (i.e., *zigzag-⊥* configuration) (see Figure S4 in the supporting information). The series of spectra in Figure 3a and 3b clearly prove a direct correlation between the magnitude of redshift (Δλ) of the resonant peak and solution concentration (Δλ is the difference between the positions of the resonant peak with the BM infiltrated with glucose solutions and with pure water).

The dependence between the magnitude of Δλ and concentration of glucose solutions is reported in Figure 3c and d for the *chiral*, *zigzag-∥* and *zigzag-⊥* configurations, either for the low (Figure 3c)) or high (Figure 3d)) concentration ranges. These plots can be taken as calibration curves of the utilized BMs. The higher slope for the *chiral* BM curve clearly proves that this BM presents the highest sensitivity for concentration analysis when using Δλ as working parameter.

From the reported values of RI of glucose solutions[43] (see Table 5 in Supporting Information) we have calculated the detection sensitivity Δλ/Δn expressed in nm over refractive index units (RIU). For the *chiral* BM, Δλ/Δn were 417 and 275 nm/RIU for low and high concentration ranges, respectively. In the case of the *zigzag*-∥ configuration the sensitivities were 248 and 137 nm/RIU for these concentration ranges, while for the *zigzag-⊥* these values were 190 and 119 nm/RIU (Table 1). From these sensitivity values, it is possible to estimate the minimum glucose concentration change detectable with the BMs depends on the photonic structure/detection method. Since the lowest wavelength change that can be followed is 0.1 nm (for our experimental set-up), the lowest detectable refractive index change is approximately 0.0005 RIU for a sensitivity 200 nm/RIU. This corresponds to approx. 2.5 gr glucose/l, i.e., 0.015 M

3.2.2 Determination of glucose concentration measuring intensity changes at a fixed wavelength of BMs' resonant peaks.

The previous analysis requires a spectrophotometer to monitor redshifts of resonant peak positions, a procedure that besides expensive can be unpractical when working with real microfluidic systems. An alternative consists of following changes in intensity at a given wavelength after infiltration with different solutions. This option would be compatible with the use of cheap intensity detectors as photodiodes, and single wavelength sources (e.g. a LED or lasers for a higher resolution) for excitation.

The quantification principle using this methodology is described in Figure 4 a) and b) for chips made with *chiral* and *zig-zag* BMs, respectively. It is apparent in Figure 4a) that due to the redshift of the resonant peak of the *chiral* BM the difference in transmittance ΔT at the

wavelength of the resonant peak maximum of the *chiral* BM infiltrated with pure water can be used as a monitoring parameter of concentration. According to Figure 4b), for the zigzag BM two parameters, ΔT∥ and ΔT⊥, can be obtained when using polarized light at ∥ or ⊥ configurations and as reference the resonant peak spectrum of the BM filled with water measured at a ∥ configuration. Each one of these two parameters permit selecting spectral zones of the resonant peak where due to the Gaussian-type shape of the resonant peak changes in transmission are maxima for either low or high concentration ranges. It is noteworthy in this regard that the wavelength chosen for evaluation was arbitrarily selected in order to yield the highest possible intensity variation for a given range of infiltrated liquid refractive index (i.e., at a wavelength where the slope of the resonant peak was maximum and where shifts in position would yield the maximum variation in transmittance).

Figure 4 c) and d) show the evolution of ΔT (*chiral* BM) and ΔT∥ and ΔT⊥ (*zig-zag* BM) with the glucose concentration. The left-blue ordinate axis refers to ΔT⊥ (*zig-zag* BM). The right-black ordinate axis refers to ΔT (*chiral* BM) and ΔT∥ (*zig-zag* BM). These graphs show that analysis sensitivity is different depending on range of concentrations, type of BM and, for the *zig-zag* BM, on measurement strategy (i.e., ΔT∥ or ΔT⊥). Defining as sensitivity parameter the ratio ΔT/Δn, approximate values for the high concentration range and the particular BM utilized for the analysis were 395%/RIU for *chiral* BM and 369 %/RIU and 272%/RIU for zig-zag BM, in this latter case for the ∥ and ⊥ configurations, respectively (Table 1). For the low concentration range these values were 440, for *chiral* BM and 432 and 671 %/RIU for *zig-zag* BMs, respectively. As in the previous strategy based on Δλ variations, the minimum glucose concentration change detectable following ΔT depends on the photonic structure/detection strategy. Since the minimum variation in this case is about 0.1%, then, for s=300%/RIU the minimum glucose concentration change corresponds to 0.0003 RIU change for the water-*glucose solution, i.e., approximately 0.01 M.*

3.2.3 Determination of glucose concentrations following changes on the polarization activity of zigzag BM.

The optical activity of the *zig-zag* BM can be modulated by liquid infiltration,[34] leading to changes in the intensity ratio of transmitted light depending on experimental configurations typically used to ascertain the ellipticity of polarized light. We used the following two configurations:

Aligned polarizers configuration: The *zig-zag* BM is placed between two polarizers with aligned transmission axes and its fence-bundling direction oriented 45^{o} off with respect to them.

Crossed polarizers configuration: The *zig-zag* BM is placed between two polarizers with crossed transmission axes and its fence-bundling direction oriented 45^{o} off with respect to them.

Figure 5 presents selected spectra recorded for the aligned and crossed configurations and increasingly higher concentrations of glucose solutions. It is apparent that besides a redshift for the two configurations, the intensity of the spectra increases/decreases for the aligned and crossed configurations, respectively. This tendency agrees with the experiment reported in ref.34 where pure liquids of increasingly higher RI were infiltrated in this type of BM. Herein, we propose that variations in the intensity ratio between the resonant peaks recorded for the crossed and aligned configurations, Δβ, can be taken as a measurement of glucose concentration. For highly concentrated solutions, the calibration curve reported in Figure 5 d) yields a clear dependence of this ratio on glucose concentration. Meanwhile, the curve in Figure

5 c), corresponding to low concentrations of glucose, suggests that the limit of detection with this methodology would be about 0.02M, i.e., about 4 gr glucose per liter. The obtained sensitivity parameters $\Delta\beta/\Delta n$ were 137 and 147 RIU^{-1} for low and high concentration ranges, respectively (Table 1).

Since $\Delta\beta$ is independent of the illumination intensity, the use of these *zig-zag* BM transducers and this measurement procedure avoids experimental problems stemming from malfunctions or time instabilities of the light source, as well as other drifts and time instabilities of the measurement system. It is also noteworthy that directly measuring the peaks areas only requires a light source for excitation around the resonant peak position (e.g., a LED) and a photodiode for detection.

3.3 Monitoring glucose solutions in reflection mode

Measurements carried out as indicated in Figure 1c) present the advantage of providing information exclusively on the liquid infiltrated in the BM without any contribution from the surrounding medium as it might happen in transmission mode. This could be a problem if the solution is colored and there is an intense absorption band due to the liquid filling the cell volume (see Figure 1a) that overlaps the resonant peak and therefore affect the measurement of $\Delta\lambda$, ΔT or $\Delta\beta$ (note that such an effect would be negligible in reflection since only the volume infiltrated in the pores is then monitored).

Figure 6 a) shows a set of resonant peak reflectance spectra recorded for the *zig-zag* BM for a set of glucose solutions of increasing concentrations (see the complete spectra in Figure S6 of the supported information). It is apparent that the spectra present a progressive redshift and that $\Delta\lambda$ and ΔT can be determined as in the transmission mode to estimate glucose concentrations (see figures 3 and 4). This analysis renders the calibration curves reported in Figures 6 b) and Figure 6 c) and the following sensitive parameters: 172 and 133 nm/RIU and 301 and 363 %/RIU for $\Delta\lambda$ and ΔT and low and high concentration ranges, respectively (Table 1).

With the device in reflection mode described in Figure 1 c) and the *zig-zag* BM we also determined the modulation of polarization activity upon liquid infiltration. Polarizers (#1) and (#2) in the scheme of Figure 1c were placed either aligned (//) or crossed (X) to each other as indicated in the scheme of Figure 7. Resonant peak spectra were recorded for this BM infiltrated with water and a series of glucose solutions (a complete spectrum is reported as supported information in Figure S7) both for the aligned and cross configurations. The spectra recorded in the aligned configuration were similar to those recorded without placing the second polarizer after the BM (c.f., spectra in Figure 6 a). The Gaussian-type shape of these spectra differs from that recorded in the crossed configuration (Figure 7 a), an effect that will not be discussed in detail here and that reflects the complex retarder behavior of the *zig-zag* BM when measured in reflection using the particular detection geometry of our device.[34] Following a strategy similar to that in Figure 5 for measurements in transmission, the ratio between the intensity of the resonant feature for the aligned and cross configurations (i.e., β', with the cross configuration intensity taken as the variation between maximum and minimum of the curves) was used to get the calibration curves in Figures 7 b) and c). Similar advantages (e.g., neglecting instability of light sources and similar effects) to those quoted above for transmission can be claimed here if working in reflection. The sensitivity parameters $\Delta\beta'/\Delta n$ calculated in this way have approximate values of 44 and 94 RIU-1 for the low and high concentration ranges respectively (Table 1).

3.4 Discussion

The use of 2D and 3D PCs to determine the RI of liquids and solutions in microfluidic systems has been amply discussed in literature[1,11–16,18–21][1,11–16,18–21]. Other methods based on plasmonic detection have also been proposed. [4-6] The summary of sensitivity parameters in Table 1 for our 1D porous BMs clearly demonstrates the possibilities of the 1D porous BM as optofluidic transducers for the analysis of glucose concentrations, with responses similar to those reported in literature for other PC-based or inverse opals procedures (although less than detection based on plasmonic effects [4,5], see supporting information Table S8). Depending on the transducer different figures of merit are used to assess their sensing capacity. A common figure of merit in plasmonic and other optical detection methods is the displacement of the resonant peak divided by its width. Herein, due to the relatively high width of the BM resonant peak we have disregarded this feature to estimate sensitivities and relay on the parameters gathered in Table 1. The reported sensitivity values in this table are well fitted for the use of the BMs in the food industry. For example, for the case of grapes wine production, the refractive index of the grape-juice solution varies by about 0.025 RIU [44] during fermentation. Since the smallest wavelength shift detected by our system is ~0.1 nm, for a transducer with a sensitivity of 200 nm/RIU, the minimum detectable change of refractive index would be 0.0005 RIU (i.e., equivalent to approximately 2.5 g glucose/l, see Table S5), which is by far small enough for this application. However, this range of sensitivity values would be not high enough for some medical applications where, for glucose determination in blood, 100 times higher sensitivities are often required.

According to Table 1 the sensitivity of measurement depends on different experimental factors such as the *chiral* or *zigzag* configuration of the BMs, the use of polarized light for the optical interrogation, the geometry of detection (either normal incidence transmission or near normal incidence reflection), the detection parameter (peak shift, peak intensity at a fixed wavelength, or intensity ratio between parallel and crossed polarizers configurations), or the concentration range of the solution. Although a systematic assessment of the reasons explaining these differences is outside the scope of this work, we can comment on microstructural and other experimental features that should be taken into account for their justification. The anisotropic optical response of BM transducers is due to their microstructural anisotropy and the preferential distribution of porosity along a given direction. Under these conditions, it is not surprising that for *zig-zag* BMs sensitivity varies with the orientation of light polarization and that different sensitivities are found when probing with light polarized parallel or perpendicular to the fence-bundling direction (in the parallel case we mostly probe liquid infiltrated in mesopores within the columns while for perpendicular polarization the probed mesopores are in-between the associated nano-columns, see schemes in Figure S1. In the light of this sample anisotropy is neither striking that the geometry of the detection affect sensitivity since for the transmission arrangement the measurements are made at normal incidence, while for the reflection arrangement, the angle of incidence is 75º with respect to the surface. Moreover, sample porosity might not be identical for the two type of BMs (*chiral* and *zigzag*) considered in this work, with the additional factor that in *chiral* BMs porosity is evenly distributed in the plane and they are interrogated with un-polarized light. It is also reasonable to assume that the change in polarizability of the infiltrated BM system may not be linear with the solution concentration. In general, we mostly obtain higher sensitivities for the lowest glucose-water concentrations

(below 0.5 M), i.e., under conditions with the highest refractive index contrast between the solutions and the materials (SiO_2, TiO_2) forming the BM.

The label-free BM transducers developed in the present work have a series of features that deserve additional comments. The manufacture procedure of this type of BMs is quite simple, just involving a one-step vacuum deposition method,[24] does not require lithography or 2D manufacturing, is compatible with any kind of substrate and permits the fabrication of a large set of chips in the same experiment. They work well for a large range of RI of solutions, enabling detection within a large range of concentrations. This capability highly contrasts with other optofluidic systems providing good results only for either low [4,5,8] or high concentration ranges.[45] In addition, the small amount of liquids required for analysis (a rough estimation of the volume of the void space in the pores of the BM renders a value smaller than 1nL per mm^2 of area) sustains their use within a lab on a chip approach in microfluidics. A high reversibility and a short response time (less than one second once the porous BM is exposed to a new liquid) are additional features supporting its use for these applications. It is also noteworthy that the label-free character of the method ensures a systematic and long-time utilization without degradation.

Another strong point of the BMs chips regarding their incorporation into microfluidic systems rely on their flexibility and the variety of interrogation methods which are compatible with their optical behavior. In this regard, it deserves stressing that the reflection mode of detection enables the analysis of any kind of liquid, even if it contains particles or cells in suspension or if it disperses the light (e.g., natural juice, milk, blood, etc.). In fact, when the BMs are interrogated in reflection mode only the liquid infiltrated in their pores contributes to the observed spectral changes. The small size of the pores, all of them in the range of nanometers (always smaller than 10 nm)[34] prevents that suspended particles/cells enters the BMs, making that the photonic information refers exclusively to the liquid without interferences from suspended particles. In Supporting information 9 we present in a Table a series of measurements taken with every-day liquids (note that in these liquids besides glucose other dissolved substances may contribute to the measured RI) proving the versatility of the nanostructured BM for liquid analysis.

The BM transducers described in this work are label free, meaning that separate information from two of more liquids in a mixture would not be accessible. However, modifications can be envisaged to incorporate chemical selectivity, for example, through the functionalization of the inner porosity of the BM transducer to make it selective to a specific compound. Work in this line is in progress in our laboratory.

4 Conclusions

Planar and highly porous anisotropic BMs with *zig-zag* and *chiral* microstructures have been successfully incorporated in an optofluidic chip that, through the infiltration of liquids, may act as RI transducers for analytical purposes. Three measurement principles have been proposed for determining the concentration of glucose solutions. Measurements have been carried out both in transmission and reflection geometries, in this latter case with the advantage that suspended nanoparticles or cells do not enter the small pores of the layered structure and do not contribute to degrade the optical performance of the system. Changes in the spectra

induced upon liquid infiltration have been analyzed by measuring both, the shift of the resonant peak and the variations in intensity at a selected wavelength. The variation of the optical activity with the RI of the infiltrated liquid in the *zig-zag* BM has proved to be a suitable and robust method for liquid analysis that can be easily integrated in real microfluidic systems using a very simple optical detection system. The sensitivities towards glucose concentration analysis determined for the various methods of interrogation essayed in the present work compare well with others obtained with more complex photonic structures. These and other operational and manufacturing advantages of the nanostructured 1D BM support their use for the optofluidic analysis of solutions in microfluidic platforms or directly by immersion in liquids when using the reflection mode of analysis.

5 Acknowledgements

We acknowledge the support of the European Regional Development Funds program (EU-FEDER), the Spanish Ministry Economy, Industry, and Competitiveness (projects 201560E055, MAT2016-79866-R, RECUPERA 2020 and Red CONSOLIDER MAT2015-69035-REDC).

References

[1] K.E. Bates, H. Lu, Optics-Integrated Microfluidic Platforms for Biomolecular Analyses, Biophys. J. 110 (2016) 1684–1697. doi:10.1016/j.bpj.2016.03.018.

[2] F. Vollmer, L. Yang, Review Label-free detection with high-Q microcavities: a review of biosensing mechanisms for integrated devices, Nanophotonics. 1 (2012) 267–291. doi:10.1515/nanoph-2012-0021.

[3] H.K. Hunt, A.M. Armani, Label-free biological and chemical sensors, Nanoscale. 2 (2010) 1544–1559. doi:10.1039/C0NR00201A.

[4] A. Stephenson-Brown, H.-C. Wang, P. Iqbal, J.A. Preece, Y. Long, J.S. Fossey, T.D. James, P.M. Mendes, Glucose selective surface plasmon resonance-based bis-boronic acid sensor, The Analyst. 138 (2013) 7140–7145. doi:10.1039/c3an01233f.

[5] H.V. Hsieh, Z.A. Pfeiffer, T.J. Amiss, D.B. Sherman, J.B. Pitner, Direct detection of glucose by surface plasmon resonance with bacterial glucose/galactose-binding protein, Biosens. Bioelectron. 19 (2004) 653–660.

[6] Z. Liu, H. Shao, G. Liu, X. Liu, H. Zhou, Y. Hu, X. Zhang, Z. Cai, G. Gu, λ3/20000 plasmonic nanocavities with multispectral ultra-narrowband absorption for high-quality sensing, Appl. Phys. Lett. 104 (2014) 081116. doi:10.1063/1.4867028.

[7] M. Yin, B. Huang, S. Gao, A.P. Zhang, X. Ye, Optical fiber LPG biosensor integrated microfluidic chip for ultrasensitive glucose detection, Biomed. Opt. Express. 7 (2016) 2067. doi:10.1364/BOE.7.002067.

[8] Poonam Sharma, Preeta Sharan, Photonic Crystal Based Ring Resonator Sensor for Detection of Glucose Concentration for Biomedical Applications, Int. J. Emerg. Technol. Adv. Eng. 4 (2014) 702–706.

[9] A. a. P. Trichet, J. Foster, N.E. Omori, D. James, P.R. Dolan, G.M. Hughes, C. Vallance, J.M. Smith, Open-access optical microcavities for lab-on-a-chip refractive index sensing, Lab. Chip. 14 (2014) 4244–4249. doi:10.1039/C4LC00817K.

[10] C.M. Rushworth, J. Davies, J.T. Cabral, P.R. Dolan, J.M. Smith, C. Vallance, Cavity-enhanced optical methods for online microfluidic analysis, Chem. Phys. Lett. 554 (2012) 1–14. doi:10.1016/j.cplett.2012.10.009.

[11] Q. Gong, X. Hu, Photonic Crystals: Principles and Applications, Pan Stanford Publishing, 2014. https://www.crcpress.com/Photonic-Crystals-Principles-and-Applications/Gong-Hu/9789814267304 (accessed October 6, 2015).

[12] H. Kurt, D.S. Citrin, Photonic crystals for biochemical sensing in the terahertz region, Appl. Phys. Lett. 87 (2005) 041108. doi:10.1063/1.1999861.

[13] R.A. Potyrailo, S.E. Hobbs, G.M. Hieftje, Optical waveguide sensors in analytical chemistry: today's instrumentation, applications and trends for future development, Fresenius J. Anal. Chem. 362 (1998) 349–373. doi:10.1007/s002160051086.

[14] P.A. Snow, E.K. Squire, P.S.J. Russell, L.T. Canham, Vapor sensing using the optical properties of porous silicon Bragg mirrors, J. Appl. Phys. 86 (1999) 1781–1784. doi:10.1063/1.370968.

[15] S. Zangooie, R. Jansson, H. Arwin, Reversible and irreversible control of optical properties of porous silicon superlattices by thermal oxidation, vapor adsorption, and liquid penetration, J. Vac. Sci. Technol. A. 16 (1998) 2901–2912. doi:10.1116/1.581438.

[16] Y. Nishijima, K. Ueno, S. Juodkazis, V. Mizeikis, Misawa, H., T. Tanimura, K. Maeda, Inverse silica opal photonic crystals for optical sensing applications, Opt. Express. 15 (2007) 12979–12988. doi:10.1364/OE.15.012979.

[17] S. Amrehn, X. Wu, T. Wagner, High-temperature stable indium oxide photonic crystals: transducer material for optical and resistive gas sensing, J. Sens. Sens. Syst. 5 (2016) 179–185. doi:10.5194/jsss-5-179-2016.

[18] D.F. Dorfner, T. Hürlimann, T. Zabel, L.H. Frandsen, G. Abstreiter, J.J. Finley, Silicon photonic crystal nanostructures for refractive index sensing, Appl. Phys. Lett. 93 (2008) 181103. doi:10.1063/1.3009203.

[19] M. Lončar, A. Scherer, Y. Qiu, Photonic crystal laser sources for chemical detection, Appl. Phys. Lett. 82 (2003) 4648–4650. doi:10.1063/1.1586781.

[20] T. Hasek, H. Kurt, D.S. Citrin, M. Koch, Photonic crystals for fluid sensing in the subterahertz range, Appl. Phys. Lett. 89 (2006) 173508. doi:10.1063/1.2369537.

[21] A.D. Falco, L. O'Faolain, T.F. Krauss, Chemical sensing in slotted photonic crystal heterostructure cavities, Appl. Phys. Lett. 94 (2009) 063503. doi:10.1063/1.3079671.

[22] R. Casquel, J.A. Soler, M. Holgado, A. López, A. Lavín, J. de Vicente, F.J. Sanza, M.F. Laguna, M.J. Bañuls, R. Puchades, Sub-micrometric reflectometry for localized label-free biosensing, Opt. Express. 23 (2015) 12544. doi:10.1364/OE.23.012544.

[23] L. González-García, G. Lozano, A. Barranco, H. Míguez, A.R. González-Elipe, TiO2–SiO2 one-dimensional photonic crystals of controlled porosity by glancing angle physical vapour deposition, J. Mater. Chem. 20 (2010) 6408–6412. doi:10.1039/C0JM00680G.

[24] A. Barranco, A. Borras, A.R. Gonzalez-Elipe, A. Palmero, Perspectives on oblique angle deposition of thin films: From fundamentals to devices, Prog. Mater. Sci. 76 (2016) 59–153. doi:10.1016/j.pmatsci.2015.06.003.

[25] J.J. Steele, A.C. van Popta, M.M. Hawkeye, J.C. Sit, M.J. Brett, Nanostructured gradient index optical filter for high-speed humidity sensing, Sens. Actuators B Chem. 120 (2006) 213–219. doi:10.1016/j.snb.2006.02.003.

[26] M.M. Hawkeye, M.J. Brett, Photonic bandgap properties of nanostructured materials fabricated with glancing angle deposition, in: 2007: pp. 683204-683204–10. doi:10.1117/12.756818.

[27] M.F. Schubert, J.-Q. Xi, J.K. Kim, E.F. Schubert, Distributed Bragg reflector consisting of high- and low-refractive-index thin film layers made of the same material, Appl. Phys. Lett. 90 (2007) 141115. doi:10.1063/1.2720269.

[28] M.F. Schubert, J.K. Kim, S. Chhajed, E.F. Schubert, Conductive distributed Bragg reflector fabricated by oblique angle deposition from a single material</title>, in: M.J. Ellison (Ed.), 2007: pp. 667403-667403–7. doi:10.1117/12.731266.

[29] K. Kaminska, K. Robbie, Birefringent Omnidirectional Reflector, Appl. Opt. 43 (2004) 1570. doi:10.1364/AO.43.001570.

[30] M. Oliva-Ramirez, L. González-García, J. Parra-Barranco, F. Yubero, A. Barranco, A.R. González-Elipe, Liquids Analysis with Optofluidic Bragg Microcavities, ACS Appl. Mater. Interfaces. 5 (2013) 6743–6750. doi:10.1021/am401685r.

[31] D.P. Singh, S.H. Lee, I.Y. Choi, J.K. Kim, Spatially graded TiO_2-SiO_2 Bragg reflector with rainbow-colored photonic band gap, Opt. Express. 23 (2015) 17568. doi:10.1364/OE.23.017568.

[32] A. Ranft, I. Pavlichenko, K. Szendrei, P.M. Zehetmaier, Y. Hu, A. von Mankowski, B.V. Lotsch, 1D photonic defect structures based on colloidal porous frameworks: Reverse pore engineering and vapor sorption, Microporous Mesoporous Mater. 216 (2015) 216–224. doi:10.1016/j.micromeso.2015.05.031.

[33] M. Anaya, A. Rubino, M. E. Calvo, H. Míguez, Solution processed high refractive index contrast distributed Bragg reflectors, J. Mater. Chem. C. 4 (2016) 4532–4537. doi:10.1039/C6TC00663A.

[34] M. Oliva-Ramirez, A. Barranco, M. Löffler, F. Yubero, A.R. González-Elipe, Optofluidic Modulation of Self-Associated Nanostructural Units Forming Planar Bragg Microcavities, ACS Nano. (2015). doi:10.1021/acsnano.5b06625.

[35] S. Wild, G. Roglic, A. Green, R. Sicree, H. King, Global prevalence of diabetes: estimates for the year 2000 and projections for 2030, Diabetes Care. 27 (2004) 1047–1053.

[36] L.V. Shkotova, N.Y. Piechniakova, O.L. Kukla, S.V. Dzyadevych, Thin-film amperometric multibiosensor for simultaneous determination of lactate and glucose in wine, Food Chem. 197 (2016) 972–978. doi:10.1016/j.foodchem.2015.11.066.

[37] R. Wilson, A.P.F. Turner, Glucose oxidase: an ideal enzyme, Biosens. Bioelectron. 7 (1992) 165–185. doi:10.1016/0956-5663(92)87013-F.

[38] J. Wang, Electrochemical Glucose Biosensors, Chem. Rev. 108 (2008) 814–825. doi:10.1021/cr068123a.

[39] Pedro Salazar, Victor Rico, Agustín R. Glez-Elipe, Nickel–copper bilayer nanoporous electrode prepared by physical vapor deposition at oblique angles for the non-enzymatic determination of glucose, Sens. Actuators B Chem. 226 (2016) 436–443.

[40] J.P.-B. Lola González-García, Correlation lengths, porosity and water adsorption in TiO_2 thin films prepared by glancing angle deposition., Nanotechnology. 23 (2012) 205701. doi:10.1088/0957-4484/23/20/205701.

[41] W. Cai, V. Shalaev, Optical Metamaterials, Springer New York, New York, NY, 2010. http://link.springer.com/10.1007/978-1-4419-1151-3 (accessed October 6, 2016).

[42] W.M. bin M. Yunus, A. bin A. Rahman, Refractive index of solutions at high concentrations, Appl. Opt. 27 (1988) 3341. doi:10.1364/AO.27.003341.

[43] D.R. Lide, CRC Handbook of Chemistry and Physics, Internet Version., CRC Press, Boca Raton, FL, 2005. http://www.hbcpnetbase.com/ (accessed October 1, 2015).

[44] F. Jimenez-Marquez, J. Vázquez, J. Ubeda, J.L. Sánchez-Rojas. Low cost and portable refractive optoelectronic device for measuring wine fermentation kinetics, Sensors and Actuators B 178 (2013) 316. doi: 10.1016/j.snb.2012.12.091

[45] L.S. Vaca-Oyola, E. Marin, J.B. Rojas-Trigos, A. Cifuentes, H. Cabrera, S. Alvarado, E. Cedeño, A. Calderón, O. Delgado-Vasallo, A liquids refractive index spectrometer, Sens. Actuators B Chem. 229 (2016) 249–256.

Table 1. Summary of sensitivity parameters determined for the BMs used for optofluidic detection under different configurations.

	Δλ/Δn (nm RIU-1) (Low/High range)		ΔT/Δn (% RIU-1) (Low/High range)			Δβ/Δn (RIU-1) (Low/High range)
Type of BM	Chiral	Zig-zag ∥	Chiral	Zig-zag ⊥	Zig-zag ∥	Zig-zag
T(%) mode	417/275	248/137	440/395	671/272	432/369	137/147
Type of BM	Zig-zag		Zig-zag			Zig-zag
R(%) mode	172/133		301/363			44/94

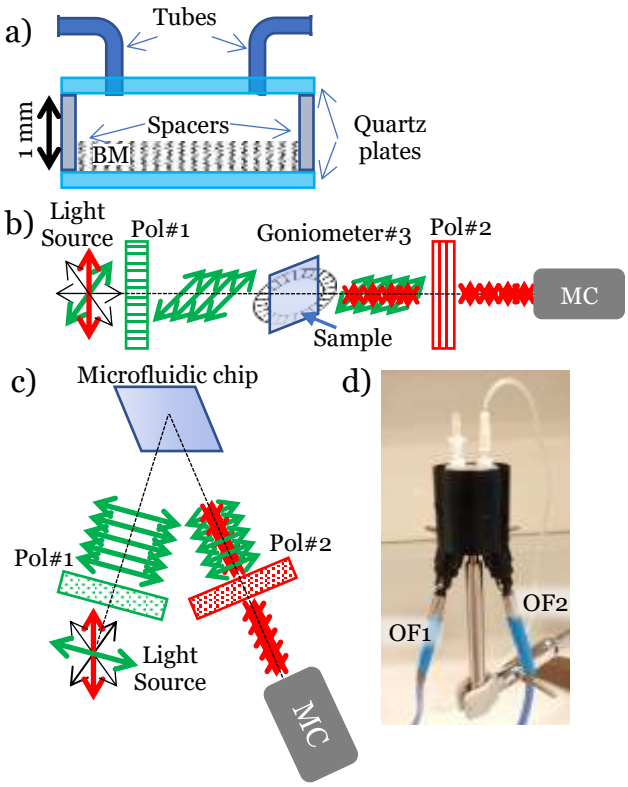

Figure 1. a) Scheme of the microfluidic chip used for analysis with indication of the inlet and outlet tubes, the observation area and the BM. The drawing is not at scale and the distance between the two plates is approximately 1 mm. b) and c) Layouts of the optical system used for the analysis in transmission and reflection: (#1, #2) polarizers which can be oriented either aligned or crossed to each other; (#3) goniometer to azimuthally rotate the chip with respect to the beam; d) Photograph of the optical set up used for the measurements in reflection. OF1 and OF2 optical fibres used for illumination and detection, respectively.

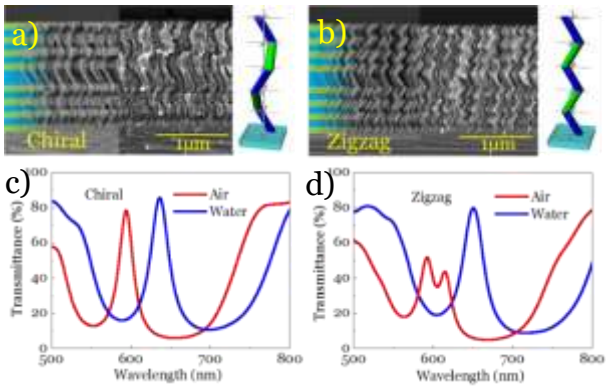

Figure 2. a) Cross-sectional SEM micrographs (BSE and SE) of a cleaved *chiral* BMs. Colours overpainted on the images highlight the layered structure. b) Ditto for a *zig-zag* BM. c) Transmission spectra recorded with unpolarised light for the *chiral* BM (red) and its optofluidic response (blue) when it was infiltrated with water. d) Ditto for a *zig-zag* BM.

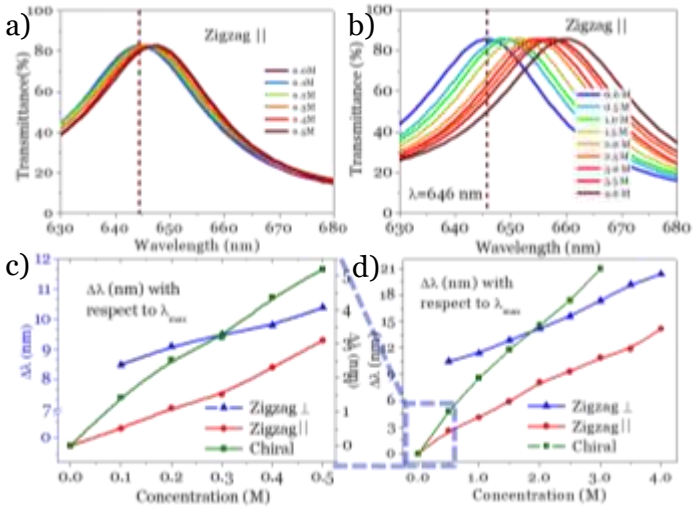

Figure 3. UV-vis transmission spectra around the resonant peak recorded in ‖ configuration for water and a series of glucose solutions of low (a) and high (b) concentrations infiltrating the *zig-zag* BM. c) Plot of the redshift Δλ of the resonant peak as a function of the glucose concentration for *chiral* and *zig-zag* BMs recorded with polarized light. d) Ditto for high concentrations of glucose. The lines are plotted to guide the eyes.

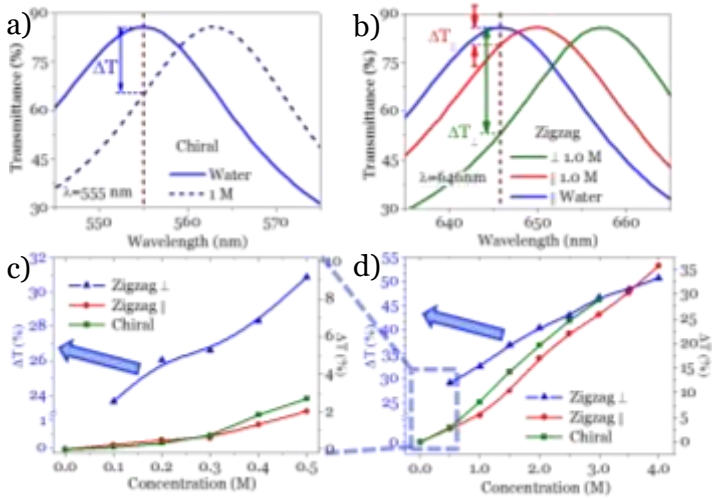

Figure 4. Measurement principle based on changes of transmitted intensity. a) Transmittance spectra around the resonant peak for a *chiral* BM infiltrated with water and a 1.0 M solution of glucose. ΔT is the difference in transmittance at the wavelength of the maximum of the resonant peak position recorded with the *chiral* BM infiltrated water taken as a reference (dashed vertical line). b) Ditto for the *zig-zag* BM. ΔT∥ is the difference in transmittance when spectra of both the reference and 1.0 M glucose solutions are recorded at a ∥ configuration. ΔT⊥ corresponds to a similar measurement with the reference spectrum recorded at a ∥ configuration and the 1.0 M glucose solution recorded at a ⊥ configuration (dashed vertical line) c) Evolution of ΔT (*chiral* BM) and ΔT∥ and ΔT⊥ (*zig-zag* BM) with the glucose concentration. d) Ditto for higher concentrations. The left-blue ordinate axis refers ΔT⊥ (*zig-zag* BM). The right-black ordinate axis refers to ΔT (*chiral* BM) and ΔT∥ (*zig-zag* BM). The lines are plotted to guide the eyes.

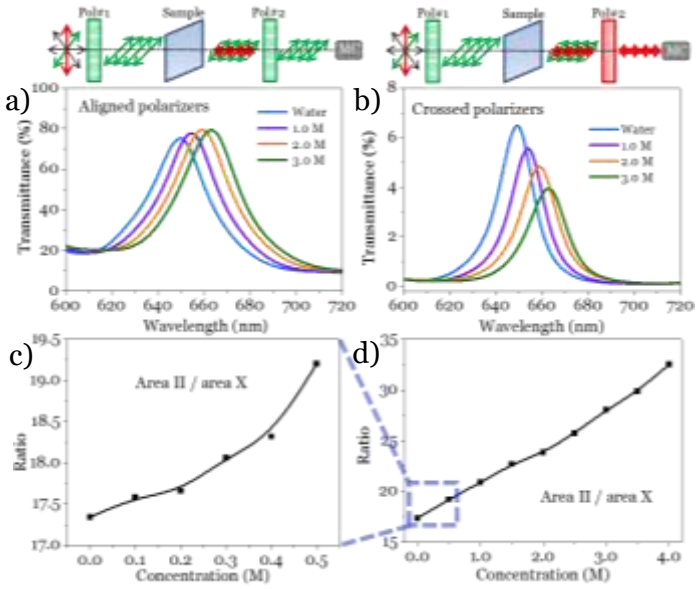

Figure 5. a) & b) Transmittance spectra recorded around the resonant peak for the *zig-zag* BM infiltrated with water and several solutions of glucose (see the difference in the scale units in each case). The sample was azimuthally rotated by 45º with respect to the polarization plane of light and placed in-between two aligned (a)) and crossed (b)) polarizers. c) Ratio between the areas of the resonant peaks recorded in aligned and crossed configuration as a function of glucose concentration. d) Ditto for higher concentrations of glucose. The lines are plotted to guide the eyes.

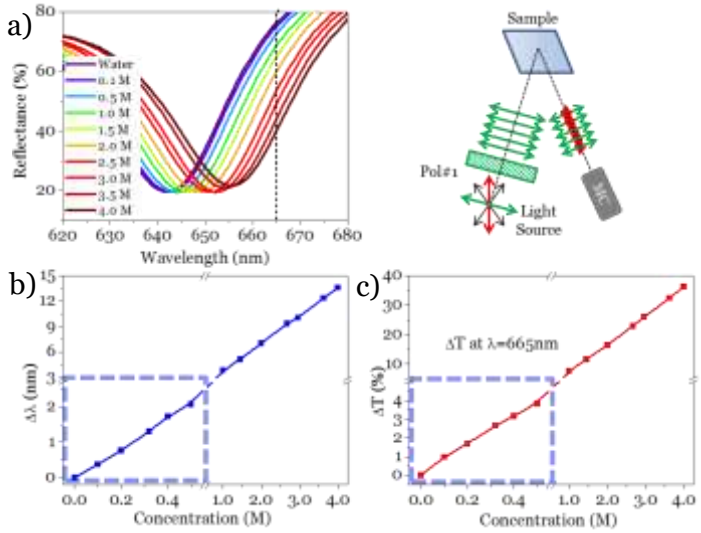

Figure 6. a) UV-vis reflectance spectra around the resonant peak for water and a series of glucose solutions infiltrating the *zig-zag* BM. The spectra were recorded with linear polarized light parallel (//) to the fence-bundling direction of the BM and forming 15º with respect to the surface normal. A scheme of the optical setup is included for clarity. Plots of the redshift of the resonant peak b) and of the evolution of the difference in transmittance c) as a function of the glucose concentration for the spectra presented in a). Note that the dashed blue square highlights a zoom in the scales of both axes.

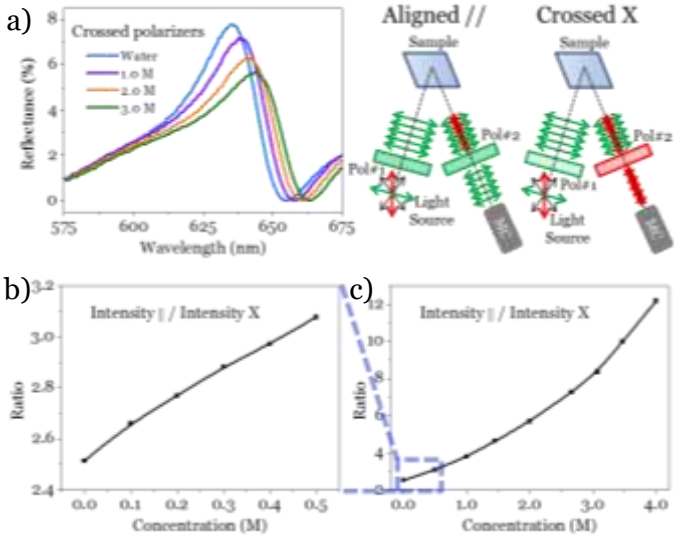

Figure 7. a) Reflectance spectra around the BM resonant peak for water and a series of glucose solutions infiltrating the *zig-zag* BM. The spectra were recorded with crossed polarizers. A scheme of the aligned (//) and crossed (X) configurations can be seen at the right of the spectra. b) Ratio between intensities of the resonant peaks of the BM recorded with aligned and crossed polarizers configuration as a function of glucose concentration (up to 0.5 M). c) Ditto for higher concentrations of glucose.

Manuel Oliva-Ramírez received his Ph.D. degree in Material Science from the University of Seville in 2016 from his work in the Institute of Material Science of Seville. His research was related to the design and fabrication of nanostructured porous thin films of different oxides for their implementation in optofluidic and photovoltaic devices. He is currently a postdoctoral researcher at the Leibniz-Institute for New Materials in Saarbruecken, and working on the development of conductive composites.

Jorge Gil-Rostra received his degree in Chemistry from de University of Burgos (Spain) in 1998. He received his Ph. D. degree in Materials Science from the University of Seville-CSIC (Spain) in 2013. From 1998 to 2007 he has worked as Responsible of Surface Treatments and Quality Manager at different Spanish companies in sectors such as construction, automotive and aeronautics. Since 2007 he worked as a researcher at the Institute of Materials Science of Seville (ICMSE-CSIC). His main research interest focus on magnetron sputtering deposition methods, mixed oxides thin films, luminescent materials and optofluidic devices.

Francisco Yubero is research scientist from the Consejo Superior de Investigaciones Científicas at the Institute of Materials Science of Seville, Spain. He received his Ph.D. degree in physics at the Universidad Autónoma de Madrid, Spain in 1993. From 1993 to 1996, he worked as a Postdoctoral Fellow at Laboratoire pour l'Utilisation du Rayonnement Electromagnétique (LURE) in Paris, France. His research focuses on theoretical aspects related to surface electron spectroscopies, and the development of practical applications of nanostructured porous thin films.

Agustín R. González-Elipe received his M.Sc. in Chemistry in 1976 (University ofSeville) and his Ph.D. in Chemistry in 1979 (University Complutense of Madrid). He is the Group Leader of the "Nanotechnology on Surface Laboratory" in the Instituto de Ciencia de Materiales de Sevilla (ICMSE) (CSIC-Univ. Seville) and expert in thin film technology and Plasma and Vacuum deposition methods, particularly in relation with the fabrication of photonic sensor films and optofluidic detection systems. He is author or co-author of more than 400 publications in SCI international journals and author and editor of several books and reviews on thin film growth and applications. He holds several international patents on these topics and has participated and directed numerous research projects funded by national and European agencies or contracted with the industry.